

ARTICLE OPEN



Significant contributions of trimethylamine to sulfuric acid nucleation in polluted environments

Runlong Cai ^{1,8}, Rujing Yin^{2,8}, Xue Li^{3,8}, Hong-Bin Xie^{3,✉}, Dongsen Yang⁴, Veli-Matti Kerminen ¹, James N. Smith⁵, Yan Ma⁴, Jiming Hao², Jingwen Chen³, Markku Kulmala ^{1,6}, Jun Zheng ^{1,6}, Jingkun Jiang ^{1,6} and Jonas Elm ^{1,7}

As one of the least understood aerosol processes, nucleation can be a dominant source of atmospheric aerosols. Sulfuric acid (SA)-amine binary nucleation with dimethylamine (DMA) has been recognized as a governing mechanism in the polluted continental boundary layer. Here we demonstrate the importance of trimethylamine (TMA) for nucleation in the complex atmosphere and propose a molecular-level SA-DMA-TMA ternary nucleation mechanism as an improvement upon the conventional binary mechanism. Using the proposed mechanism, we could connect the gaseous amines to the SA-amine cluster signals measured in the atmosphere of urban Beijing. Results show that TMA can accelerate the SA-DMA-based new particle formation in Beijing by 50–100%. Considering the global abundance of TMA and DMA, our findings imply comparable importance of TMA and DMA to nucleation in the polluted continental boundary layer, with probably higher contributions from TMA in polluted rural environments and future urban environments with controlled DMA emissions.

npj Climate and Atmospheric Science (2023)6:75 ; <https://doi.org/10.1038/s41612-023-00405-3>

INTRODUCTION

As a major source of the number concentrations of aerosols and cloud condensation nuclei in the global atmosphere, new particle formation (NPF) exerts important influences on the global climate^{1,2}. At regional and local scales, NPF provides a substantial aerosol surface area for heterogeneous physicochemical processes, plausibly contributing to haze formation and affecting human health^{3,4}. Sulfuric acid (SA) is known as the primary gaseous precursor for NPF in diverse atmospheric environments⁵. With stabilizing bases such as amines, SA nucleates and efficiently forms new particles^{6–8}, which is a governing mechanism for nucleation in the continental boundary layer^{9–12}. As suggested by laboratory and theoretical studies, many candidate bases in the complex atmosphere may participate in SA nucleation and the initial growth of stable clusters^{7,13,14}. However, a mechanistic understanding of SA-base nucleation has mainly been established based on binary acid-base systems involving a single base type. Dimethylamine (DMA) has been found to be the governing base in well-controlled laboratory systems involving SA, DMA, ammonia, and water^{6,8}, and it has been recognized as a key base for atmospheric SA nucleation^{10,11,15}. However, the SA-DMA nucleation mechanism cannot fully explain the observed NPF rate. For instance, at low DMA concentrations in urban Beijing, predictions using the SA-DMA binary mechanism tend to underestimate the concentrations of clusters containing two SA molecules¹¹, implying significant, yet underestimated, contributions from other bases. Identifying these other candidate bases is important for a comprehensive understanding of NPF in complex atmospheric environments.

Seeking other candidate bases in atmospheric nucleation requires advances in both measurements and theories. On one hand, the participation of a candidate base in atmospheric nucleation needs to be evidenced in atmospheric observations. This requires unambiguous detection of base molecules both in the gas phase and in growing clusters, which is challenging due to the interferences of many other species. On the other hand, the knowledge of SA nucleation in several isolated binary systems^{14,16,17} may not add up to the SA nucleation mechanism in the real atmosphere, as the mixture of multiple candidate bases is expected to stabilize SA clusters synergistically¹⁸. A mechanism that includes clusters consisting of multiple bases is therefore fundamental to understanding the roles of bases in atmospheric nucleation.

Considering the concentration and base strength of candidate bases, trimethylamine (TMA) is a promising species for atmospheric nucleation. As a major component of atmospheric amines¹⁹, TMA is often found in the emission sources of DMA. Compared to DMA, TMA has smaller or comparable abundances in mobile sources and residential solid fuel combustion sources, and usually higher abundances in biological sources such as animal husbandry^{20,21}. Consequently, one can expect that in various atmospheric environments, the TMA concentration can be comparable to or even higher than the DMA concentration. Laboratory experiments have shown that TMA is almost as effective as DMA in forming clusters containing two SA molecules⁷ and new particles²². This finding is also supported by theoretical studies on the formation of SA clusters containing up to two SA molecules^{17,23}. These results suggest that TMA likely contributes to atmospheric NPF. However, the role of TMA in atmospheric nucleation remains unclear and unverified, urging measurement

¹Institute for Atmospheric and Earth System Research / Physics, Faculty of Science, University of Helsinki, 00014 Helsinki, Finland. ²State Key Joint Laboratory of Environment Simulation and Pollution Control, School of Environment, Tsinghua University, 100084 Beijing, China. ³Key Laboratory of Industrial Ecology and Environmental Engineering (Ministry of Education), School of Environmental Science and Technology, Dalian University of Technology, 116024 Dalian, China. ⁴School of Environmental Science and Engineering, Nanjing University of Information Science and Technology, 210044 Nanjing, China. ⁵Chemistry Department, University of California, Irvine, CA 92697, USA. ⁶Aerosol and Haze Laboratory, Beijing Advanced Innovation Center for Soft Matter Science and Engineering, Beijing University of Chemical Technology, 100029 Beijing, China. ⁷Department of Chemistry, iClimate, Aarhus University, Langelandsgade 140, 8000 Aarhus C, Denmark. ⁸These authors contributed equally: Runlong Cai, Rujing Yin, Xue Li. [✉]email: hbxi@dlut.edu.cn; jiangjk@tsinghua.edu.cn

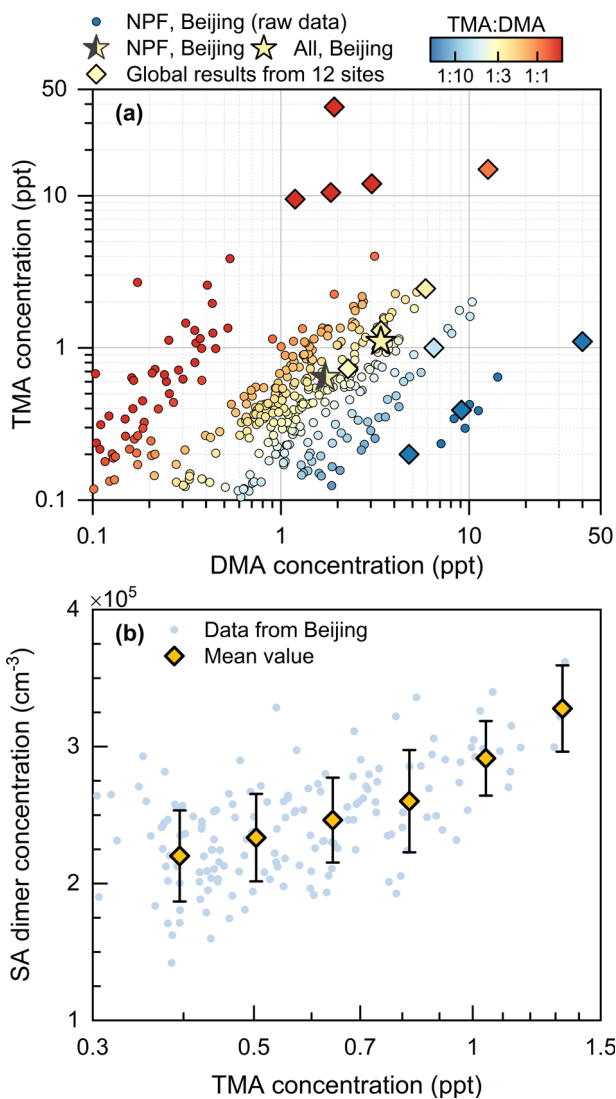


Fig. 1 TMA concentration and its association with SA clusters. **a** The measured gaseous TMA and DMA concentrations in Beijing and other environments. **b** NPF intensity indicated by the SA dimer concentration as a function of gaseous TMA concentration. In (a), the daytime NPF data for Beijing (9:00–16:00 local time) are shown in 30-min resolution. The mean TMA and DMA concentrations for NPF days and all the measurement days for urban Beijing are shown in stars. The TMA and DMA concentrations reported for 12 other global sites^{10,25–32} (see Supplementary Table S3) are shown in diamonds, covering urban, rural, coastal, and marine environments, indicating comparable TMA and DMA concentrations in diverse environments. In (b), the SA dimer concentration is used to indicate cluster and particle formation³³, and it has been scaled to the median SA dimer concentration at the amine-saturation limit (see Methods) to account for other influencing factors such as SA monomer concentration and CS. The temperature range was 280–285 K to minimize the influence of temperature on cluster evaporation. Only the data during NPF (sub-3 nm particle concentration $>10^3 \text{ cm}^{-3}$ and SA dimer concentration $>10^5 \text{ cm}^{-3}$) are shown. Data are grouped by the TMA concentration and the variation bar shows the standard deviation of each group.

evidence for its participation in atmospheric nucleation as well as improved mechanistic understanding.

Here we demonstrate that TMA is a major participant in the nucleation and initial growth of atmospheric new particles and present a molecular-level mechanism of NPF from SA, TMA, and DMA. Gaseous amines and SA-amine clusters are measured online

using advanced high-resolution chemical ionization mass spectrometry with low detection limit^{24,25}. As a major advantage over conventional chromatography methods, this state-of-the-art technique can identify atmospheric SA clusters with a fraction of constituent base molecules. Combining quantum chemical results of the stability of mixed SA-DMA-TMA clusters and cluster kinetic simulations, we show that the SA-DMA-TMA ternary nucleation mechanism can connect the gaseous amines to the SA-amine cluster signals measured in urban Beijing. We further show that TMA can on average enhance the NPF rate from SA and DMA by ~100% in Beijing and that TMA-influenced pathways can contribute ~50% to the formation of key clusters and new particles. The synergistic effects between TMA and DMA as well as the base substitution mechanism for SA-DMA-TMA nucleation are elucidated. Considering the comparable concentrations of TMA and DMA in diverse environments, these findings underline the importance of TMA to NPF in the polluted continental boundary layer, which will help to control ultrafine particles and improve climate predictions.

Following the convention introduced in Chen et al.⁹, we define an SA n-mer as a cluster containing n SA molecules and any number of base molecules. The SA n-mer concentration is correspondingly the total concentration of clusters containing n SA molecules. The cluster composition is written as $x\text{A}y\text{D}z\text{T}$, where A is SA, D is DMA, T is TMA, and x, y, z are the numbers of corresponding constituent molecules in one cluster.

RESULTS

Evidence of TMA contributions to nucleation in polluted environments

Here we present evidence from gas phase and cluster measurements to show the possible involvement of TMA in atmospheric nucleation. We conducted long-term measurements in urban Beijing and measured amines in both the gas phase and the clusters using high-resolution chemical ionization mass spectrometry (see Methods). As shown in Fig. 1a, the gaseous TMA concentration (0.1–5 ppt) measured during NPF in urban Beijing was of the same order of magnitude as the DMA concentration (0.1–15 ppt). Although the average ratio of TMA to DMA in Beijing was ~1:3, the TMA concentration sometimes exceeded that of DMA during the measurement period, especially in winter. The data reported for 12 other global sites with diverse environments^{10,25–32} show similar results that the TMA concentration was also comparable to DMA concentration and it was more abundant than DMA in certain environments. Therefore, in view of both atmospheric concentrations and the suggested efficiency of TMA in stabilizing SA clusters^{7,17}, TMA could play an important role in atmospheric SA nucleation.

The contributions of TMA to nucleation are evidenced by the relationship between gaseous TMA concentration and NPF events. Despite the challenges in directly identifying the contributions of TMA to nucleation due to other influencing factors (such as SA monomer concentration, CS, DMA concentration, and T), we found a significant positive correlation between the total concentration of SA dimers and the gaseous TMA concentration after minimizing the influence of other factors (Fig. 1b, see also Supplementary Fig. S3). Since SA dimers are key clusters for SA-amine nucleation⁸ and their concentration is commonly used as an indicator for the occurrence and intensity of NPF³³, such a correlation indicates that TMA can participate in atmospheric SA nucleation.

The contributions of TMA to nucleation are also strongly evidenced by the good association between SA-TMA clusters and NPF events. We detected high signals of SA monomers to tetramers during NPF in Beijing, demonstrating a clear nucleation and growth pattern from SA molecules to clusters (Fig. 2a). More importantly, we detected SA-TMA clusters in the form of 4A1T (Supplementary Fig. S4) that, on average, constituted half of the

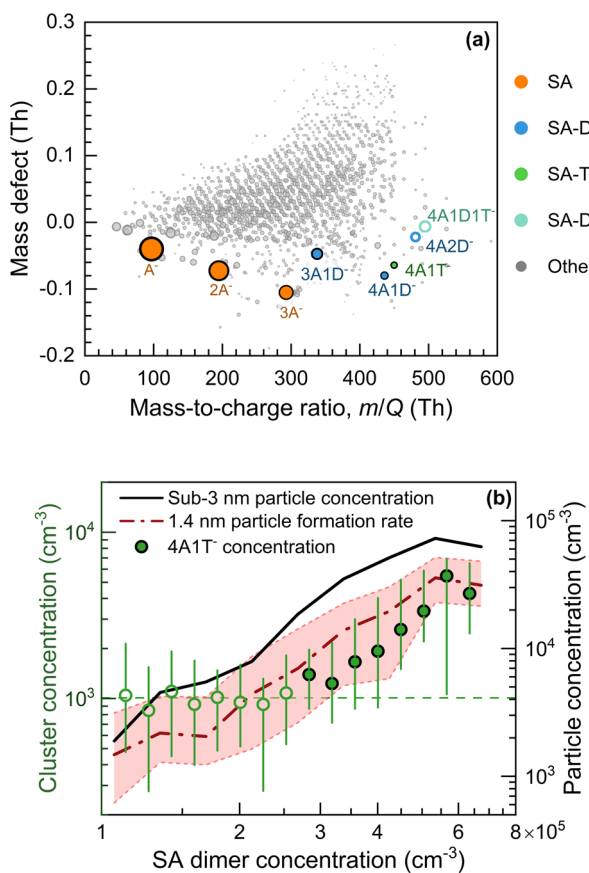


Fig. 2 The measured TMA-containing clusters and their correlation with new particle formation. **a** The measured composition and molecular weights of SA clusters. **b** The correlation between TMA-containing clusters and new particle formation. The marker size in (a) indicates the signal intensity of the detected species. SA-containing species and other species are shown in different size scales. The measured nitrate-clustered SA signals are shown as corresponding deprotonated SA signals in (a), as the nitrate ion was used to ionize SA clusters before their detection. $4A2D^-$ and $4A1D1T^-$ are shown in open markers as their signal did not correlate well with NPF. In (b), the signal of $4A1T^-$ has been converted into cluster concentration. This conversion using the calibration factor for SA monomers is likely to underestimate the cluster concentration^{8,11} yet it does not affect the increasing trend of $4A1T^-$ as a function of SA dimer concentration. The variation bar and shaded area indicate the 25th–75th percentile of the $4A1T^-$ concentration and the new particle formation rate, respectively. The dashed line indicates the background of $4A1T^-$ caused by electronic noise and the interference of isobaric peaks. The $4A1T^-$ concentration close to the background are shown in open markers.

detected SA tetramers. Figure 2b shows that the $4A1T^-$ signal was elevated as the total SA dimer concentration increased, consistent with the fact that the more TMA-containing clusters were present, the more intensive were the NPF events. The TMA-containing clusters subsequently grew into particles, resulting in the observed strong associations between the $4A1T^-$ signal and the NPF rate as well as the number concentration of freshly nucleated particles. These associations evidently indicate that TMA played a major role in the observed nucleation and growth of SA clusters, though it was not possible to measure all the stable SA-TMA clusters due to the evaporation upon ionization and cluster fragmentation during the transport process of detection^{34–36} (see the Supplementary Information for discussion in detail).

In addition to $4A1T^-$, we could also identify the $4A1D1T^-$ cluster in the measured mass spectra. $4A1D1T^-$ was plausible to exist

according to the signal assignment (Supplementary Fig. S5), even though it was difficult to determine the accurate $4A1D1T^-$ intensity due to the heavy interferences from isobaric species. In addition to the neutral clusters charged by chemical ionization upon detection as shown in Fig. 2, we could also detect naturally charged clusters. The naturally charged $5A1D1T^-$ cluster could be unambiguously identified during NPF (Supplementary Fig. S6), implying that TMA and DMA work synergistically in stabilizing SA clusters.

Although other gaseous base molecules, such as ammonia and methylamine, were also abundant in the Beijing atmosphere, TMA and DMA were the only two base molecules we were able to unambiguously detect in neutral SA clusters. We could assign the signals of clusters containing other candidate bases to the measured spectra; due to the interference of overlapping peaks, the assigned signals of these clusters were not found to be correlated with NPF characterized by particle formation rate. The DMA-containing SA clusters were detected in the form of $3A1D^-$ and $4A1D^-$, the signals of which were very similar to that of $4A1T^-$ in terms of their relationship with NPF (Supplementary Fig. S7). Since DMA is known to be a key base for SA nucleation in urban Beijing¹¹, this similarity also provides support for the importance of TMA to SA nucleation.

Mechanisms of synergistic cluster formation from SA, DMA, and TMA

The above evidence demonstrates that TMA contributes to atmospheric SA nucleation. To provide a general understanding of the TMA contributions in various environments, we present a molecular-level mechanism that includes the participation of TMA in atmospheric SA nucleation. Considering that DMA and TMA coexist in atmospheric environments, SA-DMA-TMA ternary nucleation is probed using quantum chemistry and cluster kinetics (see Methods). As shown in Fig. 3, TMA participates in SA cluster formation from the initial steps. In addition to the SA-TMA and SA-DMA pathways, the mixed SA-DMA-TMA pathway is important for cluster growth, with a dominant contribution to the growth from clusters to particles. In the presence of DMA, most SA-TMA clusters are converted into SA-DMA-TMA clusters via base substitution, though the former can also form new particles rapidly in a pure SA-TMA system (Supplementary Figs. 8–10). Consequently, TMA mainly contributes to particle formation via the mixed pathway in an SA-DMA-TMA system. In addition, the predicted abilities of SA-TMA and SA-DMA in forming SA dimers agree well with previous laboratory experiments⁷, further confirming the reliability of the employed computational method.

Contributions of TMA to cluster and particle formation

Figure 3 shows that the mixed SA-DMA-TMA pathway contributes about half of the NPF rate (characterized by the formation of clusters containing 5 or more SA molecules) under equal TMA and DMA concentrations. The contribution from the mixed pathway is found to be governed by the ratio of TMA concentration to DMA concentration (Fig. 4). Considering the TMA:DMA ratio in various environments (Fig. 1a), these results indicate the importance of TMA and the mixed SA-DMA-TMA pathway to atmospheric SA nucleation. For urban Beijing where the TMA:DMA ratio was on average 1:3, we find that the TMA-influenced pathways (i.e., the elementary reactions forming SA-TMA and SA-DMA-TMA clusters) could contribute 43% to the NPF rate, and its relative importance increased with an increasing TMA:DMA ratio (Fig. 4b). We also investigated the relative importance of TMA and DMA to cluster formation, and found that TMA is almost as efficient as DMA in an SA-DMA-TMA system. Hence, in terms of forming 1.4 nm particles, with a minor synergistic effect (enhancing factor >1, see Supplementary Figs. S11 and S12), adding TMA to an SA-DMA system is almost equivalent to adding the same amount of DMA,

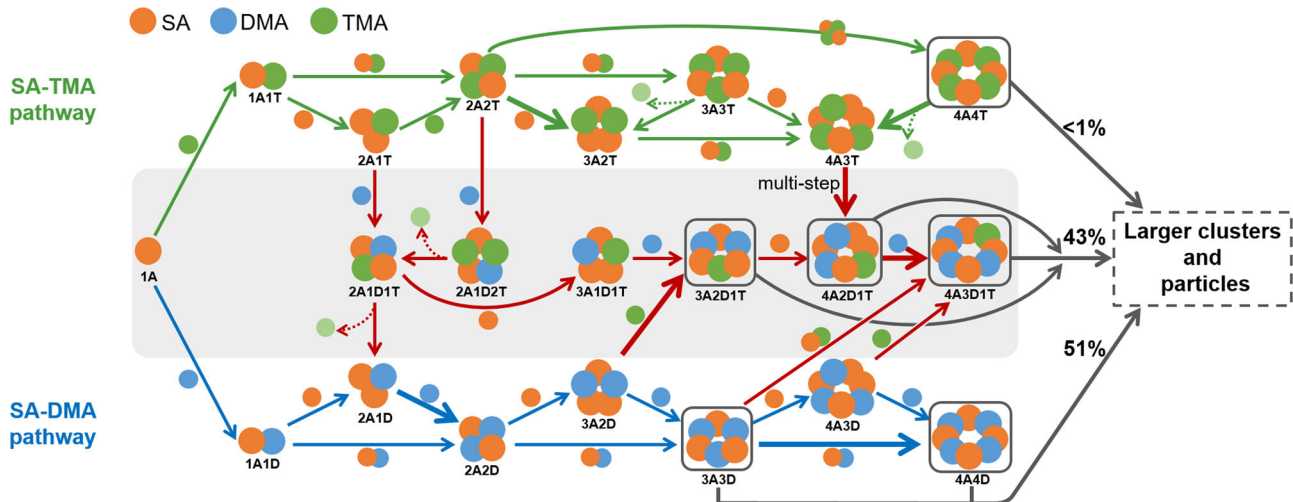


Fig. 3 A simplified schematic diagram for SA-DMA-TMA nucleation and initial growth mechanism. A, D, and T are short for sulfuric acid (SA), dimethylamine (DMA), and trimethylamine (TMA), respectively. The direction of an arrow indicates the direction of a net reaction. The thickness of an arrow indicates the relative contribution from the corresponding pathway to cluster formation. Solid and dashed arrows indicate the growth and evaporation of clusters, respectively. The shaded background indicates the mixed SA-DMA-TMA pathway. The percentages indicate the relative contributions of pathways to particle formation, characterized by the flux out of the system. Some minor contributions are not shown in this figure and hence the sum of contributions is less than 100%. The results are obtained at total SA monomer concentration = $5 \times 10^6 \text{ cm}^{-3}$, TMA concentration = 3 ppt, DMA concentration = 3 ppt, condensation sink = 0.01 s^{-1} , and temperature = 278 K.

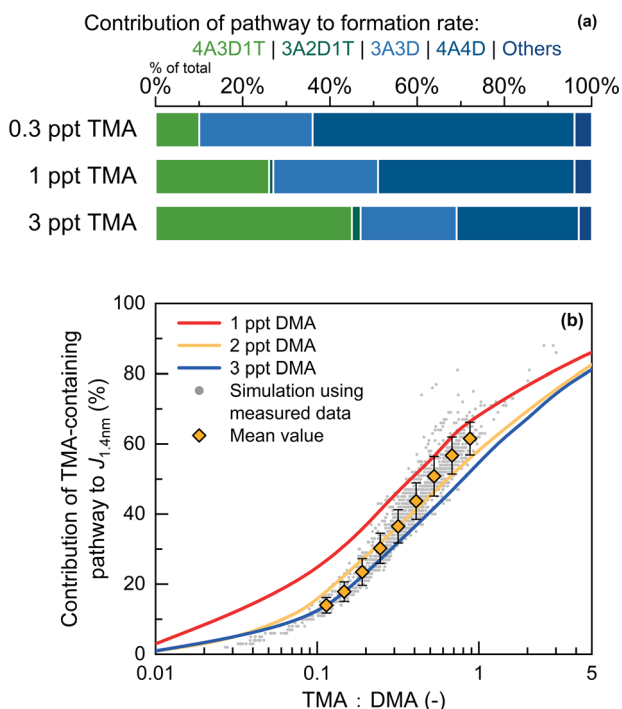


Fig. 4 The contributions of different pathways to the formation rate of $\sim 1.4 \text{ nm}$ particles ($J_{1.4\text{nm}}$). **a** shows the contributions of different pathways with 3 ppt DMA and 0.3–3 ppt TMA. **b** shows the contributions of TMA-influenced pathways. For each gray marker in **(b)**, temperature and concentration sink (CS) were obtained from measurements in Beijing. These simulation results are grouped by the TMA:DMA ratio and the orange markers and variation bars are the mean and standard deviation of each group. The horizontal stacked bars in **(a)** and the lines in **(b)** were simulated at temperature = 281 K and CS = 0.017 s^{-1} , which are medians of the measurement data. Note that the contribution from SA-DMA clusters may also involve TMA (e.g., 4A4D + 1A1T); hence the value for the TMA-influenced pathway in **(b)** is higher than the sum of contributions from SA-DMA-TMA clusters in **(a)**.

indicating that the relative concentrations of TMA and DMA govern their importance to atmospheric SA nucleation. With an average TMA:DMA = 1:3 in urban Beijing, TMA can enhance the formation rate of new particles from pure SA and DMA by 50–100% (Supplementary Fig. S13). Such enhancement is expected to be even more important in environments with higher TMA:DMA ratios (Supplementary Fig. S14). To further depict the roles of TMA in atmospheric NPF, below we quantify the contributions of TMA to the formation of key clusters.

TMA can accelerate SA nucleation by forming 1A1T clusters²³. Due to the stronger gas-phase basicity of TMA, 1A1T is more stable against evaporation than 1A1D, enabling its further growth into larger clusters before evaporation (Fig. 3). Forming the initial base-containing SA monomer (1A1B where B is a base molecule) is not only the first but also the rate-limiting step of SA-amine nucleation^{15,37–39}. This is caused by the fact that the base-containing SA monomers determine the formation rate of stable SA dimers whereas the collision between two SA molecules rarely produces a stable SA dimer. Our quantum chemical results show that an increasing TMA concentration can effectively enhance the fraction of base-containing SA monomers (Supplementary Fig. S15), and that 1A1T is the primary species (64%) of base-containing SA monomers under the same TMA and DMA concentrations.

To further validate the contributions of TMA to the formation of base-containing SA monomers, we compared the base-containing SA monomer fraction derived from the measured gaseous TMA and DMA to the fraction derived from the measured SA cluster concentrations (see Methods, Eqs. (1)–(3)). As shown in Fig. 5a, with an average TMA:DMA ratio of 1:3 in urban Beijing, TMA increased the average base-containing SA monomers fraction by 30%, better explaining the measured total SA dimer concentration than pure SA-DMA nucleation does. To reconcile the measured data in urban Beijing and laboratory experiments^{6–8}, we tuned the evaporation rates of 1A1T and 1A1D within the uncertainty range of quantum chemical results (see Methods). The 30% enhancement contributed by TMA was not sensitive to the tuned evaporation rates as the relative stability of 1A1T and 1A1D was maintained in this tuning. With the tuned cluster evaporation rates, the base-containing SA monomer fraction from the measured gaseous TMA and DMA

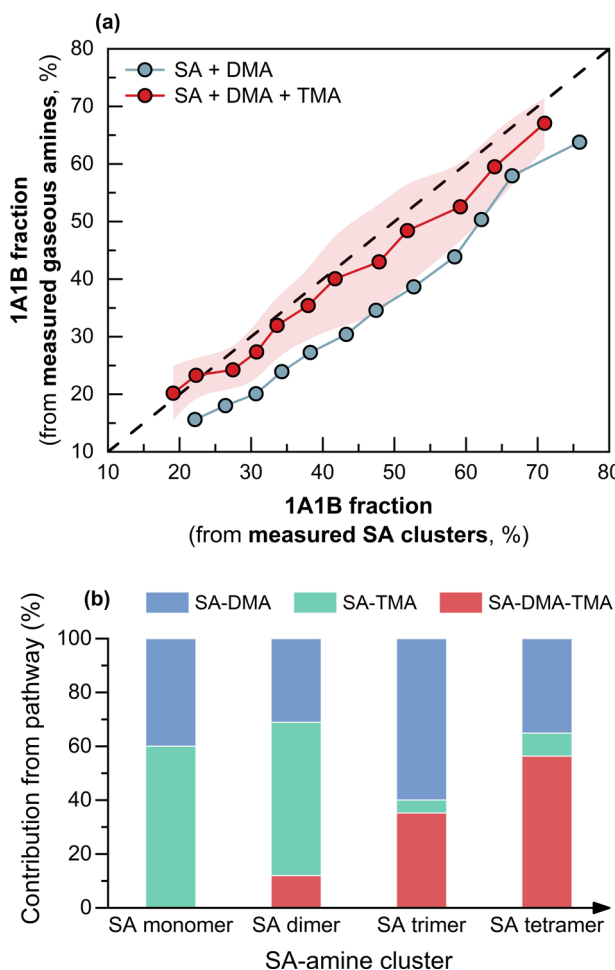


Fig. 5 The contributions of TMA to key clusters of SA nucleation. **a** Consistency between base-containing SA monomers (1A1B) explained by gaseous amines (Eq. (2)) and that derived from measured SA clusters (Eq. (3)) in urban Beijing. **b** Contributions of SA-TMA, SA-DMA, and SA-DMA-TMA pathways to the formation of SA-amine clusters. In (a), the 1A1B concentration is shown in its ratio to the total SA monomer concentration. The data are grouped by the 1A1B concentration and the shaded area indicates the variation range of the data characterized by the standard deviation. This panel shows that considering the TMA contributions can better explain the 1A1B concentration that is needed to produce the measured SA dimer concentration in urban Beijing. In (b), the contributions are computed using cluster concentrations and the fluxes for their formation at 3 ppt TMA and 3 ppt DMA.

concentrations agreed well with the one derived from the measured cluster concentrations (Fig. 5a).

The formation of stable SA dimers can be enhanced as a result of the elevated base-containing SA monomer concentration. Due to the comparatively high 1A1T fraction in SA monomers, 56% of SA dimers are formed via the SA-TMA pathway and 9% are formed via the SA-DMA-TMA pathway (Fig. 5b). The TMA-containing SA dimers can be further stabilized by base substitution and become 2A1D and 2A2D clusters, even though the former are relatively stable against evaporation, facilitating further growth from SA dimers into stable SA trimers. As shown in Fig. 5b, the contribution of the mixed pathway to cluster growth increases with an increasing cluster size. By taking into account the contributions from TMA, we could well reproduce the measured SA trimer and tetramer signals as well as their relation with NPF in urban Beijing (Supplementary Fig. S16).

DISCUSSION

Considering the concentrations of TMA in various atmospheric environments, our results imply a major role of TMA in SA-amine nucleation in a polluted continental boundary layer. Although DMA and TMA share similar emission sources, their abundances vary with the type of sources. DMA tends to be more abundant than TMA in combustion sources,²¹ TMA, in contrast, is more abundant than DMA in biological sources like animal husbandry^{20,40} and has a higher expected global average concentration¹⁹. For polluted megacities such as Beijing^{11,41}, Shanghai¹⁰, and Nanjing²⁵, DMA was reported to be on average more abundant than TMA, likely due to the higher emission of DMA from mobile sources^{21,32,42}. Hence, DMA was the governing base for nucleation in polluted megacities and TMA was a major participant. However, a decrease in DMA sources in polluted megacities can be anticipated with the control of mobile emissions in the future, whereas TMA from other sources, such as septic systems^{41,43}, may remain abundant. Consequently, the relative importance of TMA to nucleation may exceed that of DMA in future megacities. For rural environments, TMA is expected to be more abundant than DMA²⁷ due to the higher emissions of TMA from animal husbandry^{20,40}. Considering that regional NPF events usually occur over spatial extents covering tens to hundreds of kilometers^{44,45}, it is reasonable to anticipate a major contribution from TMA to regional SA-amine nucleation. This implies the importance of TMA to global climate prediction, and that controlling the emissions of TMA is a plausible solution to reducing secondary aerosol formation in the polluted continental boundary layer.

Because of the complexity of candidate bases for SA-base nucleation in the polluted continental boundary layer, it is of utmost importance to find the key bases for nucleation and obtain a holistic understanding of the atmospheric SA-base nucleation mechanism. Here we have shown that, as an abundant amine in the global atmosphere, TMA can be a major participant in nucleation in addition to DMA. This is evidenced by the detected TMA signals in growing SA clusters in urban Beijing and its close association with NPF. We propose a molecular-level mechanism of SA-DMA-TMA ternary nucleation as an improvement upon the conventional SA-DMA binary nucleation, better explaining the measured gaseous amines and SA-amine signals. With equal TMA and DMA concentrations, TMA can contribute more than 50% to the formation of base-containing SA monomers, which are key clusters to SA nucleation. These base-containing SA monomers further grow with a synergy between TMA and DMA. With on average 1/3 the concentration of DMA in urban Beijing, TMA can enhance the average NPF rate by ~50–100%, and the TMA-influenced pathways can contribute 43% to the NPF rate. These results indicate comparable importance between TMA and DMA to SA nucleation in the polluted continental boundary layer, and that TMA is expected to be the governing base in environments with high TMA emissions such as in some polluted rural atmospheres with high biological emissions.

METHODS

Measurements

Long-term field measurements were conducted at the west campus of Beijing University of Chemical Technology ($39^{\circ}44'N$, $116^{\circ}30'E$). This sampling site was located ~550 m away from the 3rd Ring Road of Beijing and the sampling inlets were on the top floor of an ~20-m-high office building. Details of the sampling site can be found in our previous studies^{36,46,47}. We used measurements from two periods, covering Jan. 23–Apr. 13, 2018 and Oct. 17, 2018–Jan 19, 2019.

Gaseous sulfuric acid (SA) and neutral clusters were measured using a chemical ionization atmospheric pressure interface high-resolution time-of-flight mass spectrometer (CI-API-TOF, Aerodyne

Research, Inc.)^{24,48}. Nitrate ion (NO_3^-) and its clusters [$(\text{HNO}_3)_{1-2}\text{NO}_3^-$] were used as the reagent ions to ionize gaseous SA and neutral clusters. The mass resolution of two Cl-API-TOF was ~8000 and ~4000, respectively, during the first (Jan. 23–Apr. 13, 2018) and second (Oct. 17, 2018–Jan 19, 2019) measurement periods. These two Cl-API-TOF were operated at similar configurations. The nitric acid vapor was volatilized from a glass tube and carried by nitrogen gas with a standard volumetric flow rate of $3 \text{ cm}^3 \text{ s}^{-1}$, then it was mixed with zero air of 20 L min^{-1} and exposed to soft X-ray to produce $(\text{HNO}_3)_{0-2}\text{NO}_3^-$. Ambient air was sampled from the window through a 1.4 m long 3/4 inch stainless steel tube. The sample flow rate of the Cl-API-TOF was 8.8 L min^{-1} , of which 0.8 L min^{-1} sample flow was analyzed by the TOF module and 8 L min^{-1} was a bypass flow. After mixing the sample flow with reagent ions, the ion-molecule reaction time within the Cl-inlet was ~0.2 s. The sensitivity to SA and the mass-dependent transmission efficiency were calibrated according to the methods described in Kürten et al.⁴⁹ and Heinritzi et al.⁵⁰, respectively. Specifically, the quantification of neutral SA clusters considers both the sensitivity to SA and the transmission efficiency.

In addition to neutral clusters charged by chemical ionization, we also measured naturally charged clusters using an atmospheric pressure interface high-resolution time-of-flight mass spectrometer (API-TOF, Tofwerk AG)⁴⁸. Ambient air was sampled to the API-TOF through a 1.4 m long 1/4 inch stainless steel tube. The sample flow of API-TOF was 3.8 L min^{-1} , of which 0.8 L min^{-1} sample flow was analyzed by the TOF module and 3 L min^{-1} was a bypass flow.

Gaseous amines were measured using a modified time-of-flight chemical ionization mass spectrometer (ToF-CIMS, Aerodyne Research, Inc.)²⁵. Water-clustered hydronium ions [$(\text{H}_2\text{O})_{1-3}\text{H}_3\text{O}^+$] were used as the reagent ions. Compared with a typical ToF-CIMS, the original ion-molecular reaction chamber was replaced with a custom-made drift-tube reactor and a corona discharge ion source in this modified ToF-CIMS. The sample flow was 6.1 L min^{-1} . The gases were sampled by a 1.5 m long 14.3 mm Teflon tube, and the tube was heated to ~60 °C to reduce the sampling loss. The mass resolution of the modified ToF-CIMS was ~4000. Compared to offline methods for measuring amines based on gas chromatography^{27,29,51}, ion chromatography^{21,30,52}, and high-performance liquid chromatography, the online method based on mass spectrometry has higher time resolution and lower detection limits.

Particle size distributions in the size range of 1 nm–10 μm were measured using a diethylene glycol scanning mobility particle sizer (DEG-SMPS)⁵³ and a particle size distribution system (PSD)⁵⁴. The DEG-SMPS and the PSD measured particles in the size range of 1–7.5 nm and 3 nm–10 μm, respectively. The DEG-SMPS sampled aerosols via the core of a sampling inlet to improve the sampling efficiency⁵⁵. A miniature cylindrical differential mobility analyzer was deployed to the DEG-SMPS to facilitate aerosol size classification⁵⁶. The PSD was sampled downstream of a PM_{10} cyclone on the roof. Details of the configuration could be found in our previous studies^{56,57}.

The formation rate of 1.4 nm (electrical mobility diameter) particles was retrieved from the measured aerosol size distributions using a population balance formula for polluted environments⁵⁸. The value of condensation sink (CS) was computed using measured aerosol number-size distributions⁵⁹. The total SA dimer concentration at the amine-saturation limit was obtained from cluster kinetic simulations with 1000-ppt amines (Supplementary Fig. S17), which could also be approximated by Eq. (1) with a negligible uncertainty (<1%),

$$\Sigma[(\text{SA})_2]_{\text{AS}} = \frac{0.5\beta_{11}(\Sigma[(\text{SA})_1])^2}{\text{CS} + \beta_{12}\Sigma[(\text{SA})_1]} \quad (1)$$

where $\Sigma[(\text{SA})_1]$ is the total concentration of SA monomers; $\Sigma[(\text{SA})_2]_{\text{AS}}$ is the total concentration of SA dimers at the amine-saturation limit; β_{11} is the collision coefficient between two SA

monomers; and β_{12} is the collision coefficient between one SA monomer and one SA dimer. We also accounted for the influence of the van der Waals attraction force on collision^{60,61}, which increases the collision coefficient by a multiplicative factor of ~2.3 and the CS by ~1.3. This equation indicates that at the amine-saturation limit every collision between two SA monomers produces a stable SA dimer, which grows into a larger cluster or is scavenged by coagulation with negligible evaporation of SA molecules. The analysis using $\Sigma[(\text{SA})_2]_{\text{AS}}$ are illustrated in detail in the Supplementary Information.

With a certain amine concentration, the base-containing SA monomer fraction can be simulated by numerically solving cluster population equations. Alternatively, it can be theoretically predicted using Eq. (2)³³,

$$\frac{\Sigma[1\text{A}1\text{B}]}{\Sigma[(\text{SA})_1]} = 1 - \frac{1}{1 + \sum_B \frac{\beta_{AB}[\text{B}]}{\text{CS} + \gamma_{1\text{A}1\text{B}}}} \quad (2)$$

where $\Sigma[1\text{A}1\text{B}]$ is the total concentration of base-containing SA monomers, B is a certain base (TMA or DMA in this study), and γ is the cluster evaporation rate. The $\beta_{AB}[\text{B}]$ term characterizes the formation rate of 1A1B. The CS and $\gamma_{1\text{A}1\text{B}}$ terms characterize the loss rates of 1A1B due to coagulation scavenging and evaporation, respectively. The losses of 1A1B by its clustering with other clusters are reasonably neglected herein as they are much smaller than $\gamma_{1\text{A}1\text{B}}$ and CS.

The base-containing SA monomer concentration can also be derived from the total SA dimer concentration using Eq. (3)³³,

$$\frac{\Sigma[1\text{A}1\text{B}]}{\Sigma[(\text{SA})_1]} = 1 - \sqrt{1 - \frac{\Sigma[(\text{SA})_2]}{\Sigma[(\text{SA})_2]_{\text{AS}}}} \quad (3)$$

where $\Sigma[(\text{SA})_2]$ is the measured total concentration of SA dimers. The accuracy of Eq. (3) for the atmospheric conditions in urban Beijing has been verified using cluster kinetic simulations.

The systematic uncertainty of the measured total SA monomer concentration associated with calibration was estimated to be less than +100%/-50%^{24,49}. The measured total SA dimer concentration was likely to be underestimated due to the uncertainties in ionization and detection, yet it does not affect our conclusions. We corrected this underestimation for the Beijing dataset with a multiplicative factor of ~1.3, which was consistent with the value reported in a laboratory study⁸. The corrected total SA dimer concentration shared a similar systematic uncertainty with the total SA monomer concentration, and comparing a measured total dimer concentration with its corresponding theoretical amine-saturation limit canceled out a part of this systematic uncertainty. The uncertainty of CS was estimated to be +10%/-10%, which was mainly propagated from the uncertainties in aerosol size distribution measurements⁶². The uncertainty of measured formation rate of 1.4 nm particles was +100%/-50%.

Simulation

Quantum chemistry and cluster kinetics were employed to probe cluster formation from the binary SA-TMA, SA-DMA and the ternary SA-DMA-TMA systems. The simulation domain covers SA-TMA, SA-DMA, and SA-DMA-TMA clusters containing up to 4 SA molecules per cluster. The structure of some clusters were obtained from previous studies^{23,63–65} and re-optimized. The structures of the remaining clusters with global minimum Gibbs free energy were identified using a multi-step sampling scheme^{64,66–69} (see the Supplementary Information). Based on the cluster structure (Supplementary Figs. S15 and S16), the standard formation Gibbs free energy of a cluster was determined as the sum of single-point energy at the DLPNO-CCSD(T)/aug-cc-pVTZ level of theory and the Gibbs free energy correction at the wB97X-D/6-31+ + G(d,p) level of theory. The standard reaction Gibbs free energy (i.e., binding free energy, ΔG) at 298.15 K for

each cluster (Supplementary Table S1) was obtained by subtracting the standard Gibbs free energy of the constituent monomers (SA, DMA, TMA) from that of the cluster. The ΔG values at other temperatures were calculated with a reasonable approximation that standard enthalpy change and standard entropy change stay constant within the studied temperature range (267.65 – 298.15 K). To validate this approximation, we employed the GoodVibes code⁷⁰ to provide more accurate values. As expected, there was a negligible difference in ΔG (0.0007–0.0478 kcal mol⁻¹) between our results and the GoodVibes results (Supplementary Table S2).

The cluster formation mechanisms and steady-state concentrations were investigated using the atmospheric cluster dynamics code (ACDC), which computes cluster evaporation rates using cluster collision rates and ΔG and performs kinetic simulations of the time-dependent cluster concentrations^{67,68}. When calculating the cluster collision coefficients and the CS, we accounted for the contribution of the van der Waals attraction force using an enhancement factor⁶¹ of 2.3 for cluster-cluster collision and 1.3 for the CS. Clusters with 5 constituent SA molecules were selected as boundary clusters for the simulation system, and their electrical mobility diameter was estimated to be ~1.4 nm^{71,72}. For dealing with non-boundary clusters growing out of the system, a higher base strength is set for TMA, compared to DMA in the ACDC simulation. In addition, it was found two unreasonable pathways (4A4D + 1 T → boundary → 4A3D1T, 4A3D1T + 1 T → boundary → 4A2D2T) by checking the cluster formation pathway since the “returned cluster” is less stable than the “growing-out cluster” in these pathways. Therefore, we forbid these two pathways to make ACDC result reasonable.

We also performed an ACDC simulation test with higher stability against evaporation of the key 1A1D and 1A1T clusters for cluster formation in the SA-DMA-TMA system, with the evaporation rates of other clusters unchanged. The higher stability is achieved by decreasing the ΔG values for forming 1A1D and 1A1T clusters by 1 kcal mol⁻¹, which is within the uncertainty range of the DLPNO-CCSD(T)/aug-cc-pVTZ method for cluster free energy calculation.

DATA AVAILABILITY

The Gibbs free energy for cluster formation can be found in the SI. The measurement data are available upon request from the corresponding authors.

CODE AVAILABILITY

The atmospheric cluster dynamics code and data processing codes are available upon request from the corresponding authors.

Received: 30 November 2022; Accepted: 16 June 2023;

Published online: 27 June 2023

REFERENCES

- Kuang, C., McMurry, P. H. & McCormick, A. V. Determination of cloud condensation nuclei production from measured new particle formation events. *Geophys. Res. Lett.* **36**, L09822 (2009).
- Gordon, H. et al. Causes and importance of new particle formation in the present-day and preindustrial atmospheres. *J. Geophys. Res. Atmos.* **122**, 8739–8760 (2017).
- Guo, S. et al. Elucidating severe urban haze formation in China. *Proc. Natl Acad. Sci. USA* **111**, 17373–17378 (2014).
- Kulmala, M. et al. Is reducing new particle formation a plausible solution to mitigate particulate air pollution in Beijing and other Chinese megacities? *Faraday Discuss.* **226**, 334–347 (2021).
- Kuang, C., McMurry, P. H., McCormick, A. V. & Eisele, F. L. Dependence of nucleation rates on sulfuric acid vapor concentration in diverse atmospheric locations. *J. Geophys. Res.* **113**, D10209 (2008).
- Almeida, J. et al. Molecular understanding of sulphuric acid-amine particle nucleation in the atmosphere. *Nature* **502**, 359–363 (2013).
- Jen, C. N., McMurry, P. H. & Hanson, D. R. Stabilization of sulfuric acid dimers by ammonia, methylamine, dimethylamine, and trimethylamine. *J. Geophys. Res. Atmos.* **119**, 7502–7514 (2014).
- Kürten, A. et al. Neutral molecular cluster formation of sulfuric acid-dimethylamine observed in real time under atmospheric conditions. *Proc. Natl Acad. Sci. USA* **111**, 15019–15024 (2014).
- Chen, M. et al. Acid-base chemical reaction model for nucleation rates in the polluted atmospheric boundary layer. *Proc. Natl Acad. Sci. USA* **109**, 18713–18718 (2012).
- Yao, L. et al. Atmospheric new particle formation from sulfuric acid and amines in a Chinese megacity. *Science* **361**, 278–281 (2018).
- Cai, R. et al. Sulfuric acid-amine nucleation in urban Beijing. *Atmos. Chem. Phys.* **21**, 2457–2468 (2021).
- Brean, J. et al. Open ocean and coastal new particle formation from sulfuric acid and amines around the Antarctic Peninsula. *Nat. Geosci.* **14**, 383–388 (2021).
- Jen, C. N., Bachman, R., Zhao, J., McMurry, P. H. & Hanson, D. R. Diamine-sulfuric acid reactions are a potent source of new particle formation. *Geophys. Res. Lett.* **43**, 867–873 (2016).
- Mylllys, N. et al. Role of base strength, cluster structure and charge in sulfuric-acid-driven particle formation. *Atmos. Chem. Phys.* **19**, 9753–9768 (2019).
- Cai, R. et al. The missing base molecules in atmospheric acid-base nucleation. *Natl Sci. Rev* **9**, nwac137 (2022).
- Ortega, I. K. et al. From quantum chemical formation free energies to evaporation rates. *Atmos. Chem. Phys.* **12**, 225–235 (2012).
- Olenius, T. et al. New particle formation from sulfuric acid and amines: Comparison of monomethylamine, dimethylamine, and trimethylamine. *J. Geophys. Res. Atmos.* **122**, 7103–7118 (2017).
- Mylllys, N., Chee, S., Olenius, T., Lawler, M. & Smith, J. Molecular-level understanding of synergistic effects in sulfuric acid-amine-ammonia mixed clusters. *J. Phys. Chem. A* **123**, 2420–2425 (2019).
- Yu, F. & Luo, G. Modeling of gaseous methylamines in the global atmosphere: impacts of oxidation and aerosol uptake. *Atmos. Chem. Phys.* **14**, 12455–12464 (2014).
- Ge, X., Wexler, A. S. & Clegg, S. L. Atmospheric amines – Part I. A review. *Atmos. Environ.* **45**, 524–546 (2011).
- Feng, X. et al. Outbreaks of ethyl-amines during haze episodes in North China Plain: a potential source of amines from ethanol gasoline vehicle emission. *Environ. Sci. Technol. Lett.* **9**, 306–311 (2022).
- Erupe, M. E., Viggiano, A. A. & Lee, S. H. The effect of trimethylamine on atmospheric nucleation involving H2SO4. *Atmos. Chem. Phys.* **11**, 4767–4775 (2011).
- Elm, J. & Clusteromics, I. principles, protocols, and applications to sulfuric acid-base cluster formation. *ACS Omega* **6**, 7804–7814 (2021).
- Jokinen, T. et al. Atmospheric sulphuric acid and neutral cluster measurements using CI-API-TOF. *Atmos. Chem. Phys.* **12**, 4117–4125 (2012).
- Zheng, J. et al. Measurement of atmospheric amines and ammonia using the high resolution time-of-flight chemical ionization mass spectrometry. *Atmos. Environ.* **102**, 249–259 (2015).
- Van Neste, A., Duce, R. A. & Lee, C. Methylamines in the marine atmosphere. *Geophys. Res. Lett.* **7**, 711–714 (1987).
- Grönberg, L., Lövkvist, P. & Jönsson, J. Å. Determination of aliphatic amines in air by membrane enrichment directly coupled to a gas chromatograph. *Chromatographia* **33**, 77–82 (1992).
- Gibb, S. W., Mantoura, R. F. C. & Liss, P. S. Ocean-atmosphere exchange and atmospheric speciation of ammonia and methylamines in the region of the NW Arabian Sea. *Glob. Biogeochem. Cycles* **13**, 161–178 (1999).
- Schade, G. W. & Crutzen, P. J. Emission of aliphatic amines from animal husbandry and their reactions: potential source of N2O and HCN. *J. Atmos. Chem.* **22**, 319–346 (1995).
- VandenBoer, T. C. et al. Ion chromatographic separation and quantitation of alkyl methylamines and ethylamines in atmospheric gas and particulate matter using preconcentration and suppressed conductivity detection. *J. Chromatogr. A* **1252**, 74–83 (2012).
- Chen, D. et al. Mapping gaseous dimethylamine, trimethylamine, ammonia, and their particulate counterparts in marine atmospheres of China's marginal seas – Part 1: Differentiating marine emission from continental transport. *Atmos. Chem. Phys.* **21**, 16413–16425 (2021).
- Chang, Y. et al. Nonagricultural emissions dominate urban atmospheric amines as revealed by mobile measurements. *Geophys. Res. Lett.* **49**, e2021GL097640 (2022).
- Cai, R. et al. An indicator for sulfuric acid-amine nucleation in atmospheric environments. *Aerosol Sci. Technol.* **55**, 1059–1069 (2021).
- Kurtén, T. et al. The effect of H2SO4 – amine clustering on chemical ionization mass spectrometry (CIMS) measurements of gas-phase sulfuric acid. *Atmos. Chem. Phys.* **11**, 3007–3019 (2011).
- Zapadinsky, E., Passananti, M., Mylllys, N., Kurten, T. & Vehkamaki, H. Modeling on fragmentation of clusters inside a mass spectrometer. *J. Phys. Chem. A* **123**, 611–624 (2019).

36. Yin, R. et al. Acid-base clusters during atmospheric new particle formation in urban Beijing. *Environ. Sci. Technol.* **55**, 10994–11005 (2021).
37. Olenius, T., Kupiainen-Maatta, O., Ortega, I. K., Kurten, T. & Vehkamaki, H. Free energy barrier in the growth of sulfuric acid-ammonia and sulfuric acid-dimethylamine clusters. *J. Chem. Phys.* **139**, 084312 (2013).
38. Elm, J. Elucidating the limiting steps in sulfuric acid-base new particle formation. *J. Phys. Chem. A* **121**, 8288–8295 (2017).
39. Chee, S., Barsanti, K., Smith, J. N. & Myllys, N. A predictive model for salt nanoparticle formation using heterodimer stability calculations. *Atmos. Chem. Phys.* **21**, 11637–11654 (2021).
40. Sintermann, J. et al. Trimethylamine emissions in animal husbandry. *Bio-geosciences* **11**, 5073–5085 (2014).
41. Zhu, S. et al. Observation and source apportionment of atmospheric alkaline gases in urban Beijing. *Environ. Sci. Technol.* **56**, 17545–17555 (2022).
42. Yang, D. et al. Emissions of ammonia and other nitrogen-containing volatile organic compounds from motor vehicles under low-speed driving conditions. *Environ. Sci. Technol.* **56**, 5440–5447 (2022).
43. Chang, Y. et al. Discovery of a potent source of gaseous amines in urban China. *Environ. Sci. Technol. Lett.* **8**, 725–731 (2021).
44. Kulmala, M. et al. Measurement of the nucleation of atmospheric aerosol particles. *Nat. Protoc.* **7**, 1651–1667 (2012).
45. Wang, Z. B. et al. Characteristics of regional new particle formation in urban and regional background environments in the North China Plain. *Atmos. Chem. Phys.* **13**, 12495–12506 (2013).
46. Liu, Y. et al. Continuous and comprehensive atmospheric observations in Beijing: a station to understand the complex urban atmospheric environment. *Big Earth Data* **4**, 295–321 (2020).
47. Deng, C. et al. Seasonal characteristics of new particle formation and growth in urban Beijing. *Environ. Sci. Technol.* **54**, 8547–8557 (2020).
48. Junninen, H. et al. A high-resolution mass spectrometer to measure atmospheric ion composition. *Atmos. Meas. Tech.* **3**, 1039–1053 (2010).
49. Kürten, A., Rondo, L., Ehrhart, S. & Curtius, J. Calibration of a chemical ionization mass spectrometer for the measurement of gaseous sulfuric acid. *J. Phys. Chem. A* **116**, 6375–6386 (2012).
50. Heinritzi, M. et al. Characterization of the mass-dependent transmission efficiency of a CIMS. *Atmos. Meas. Tech.* **9**, 1449–1460 (2016).
51. Akyüz, M. Simultaneous determination of aliphatic and aromatic amines in indoor and outdoor air samples by gas chromatography-mass spectrometry. *Talanta* **71**, 486–492 (2007).
52. Dawson, M. L. et al. Measurement of gas-phase ammonia and amines in air by collection onto an ion exchange resin and analysis by ion chromatography. *Atmos. Meas. Tech.* **7**, 2733–2744 (2014).
53. Jiang, J., Chen, M., Kuang, C., Attoui, M. & McMurry, P. H. Electrical mobility spectrometer using a diethylene glycol condensation particle counter for measurement of aerosol size distributions down to 1 nm. *Aerosol Sci. Technol.* **45**, 510–521 (2011).
54. Liu, J., Jiang, J., Zhang, Q., Deng, J. & Hao, J. A spectrometer for measuring particle size distributions in the range of 3 nm to 10 μm . *Front. Environ. Sci. Eng.* **10**, 63–72 (2016).
55. Fu, Y., Xue, M., Cai, R., Kangasluoma, J. & Jiang, J. Theoretical and experimental analysis of the core sampling method: reducing diffusional losses in aerosol sampling line. *Aerosol Sci. Technol.* **53**, 793–801 (2019).
56. Cai, R., Chen, D.-R., Hao, J. & Jiang, J. A miniature cylindrical differential mobility analyzer for sub-3 nm particle sizing. *J. Aerosol Sci.* **106**, 111–119 (2017).
57. Deng, C. et al. Seasonal characteristics of new particle formation and growth in urban Beijing. *Environ. Sci. Technol.* **54**, 8547–8557 (2020).
58. Cai, R. & Jiang, J. A new balance formula to estimate new particle formation rate: reevaluating the effect of coagulation scavenging. *Atmos. Chem. Phys.* **17**, 12659–12675 (2017).
59. Kulmala, M. et al. On the formation, growth and composition of nucleation mode particles. *Tellus* **53**, 479–490 (2001).
60. Sceats, M. G. Brownian coagulation in aerosols—the role of long range forces. *J. Colloid Interface Sci.* **129**, 105–112 (1989).
61. Stolzenburg, D. et al. Enhanced growth rate of atmospheric particles from sulfuric acid. *Atmos. Chem. Phys.* **20**, 7359–7372 (2020).
62. Wiedensohler, A. et al. Mobility particle size spectrometers: harmonization of technical standards and data structure to facilitate high quality long-term observations of atmospheric particle number size distributions. *Atmos. Meas. Tech.* **5**, 657–685 (2012).
63. Paasonen, P. et al. On the formation of sulphuric acid – amine clusters in varying atmospheric conditions and its influence on atmospheric new particle formation. *Atmos. Chem. Phys.* **12**, 9113–9133 (2012).
64. Xie, H. B. et al. Atmospheric fate of monoethanolamine: enhancing new particle formation of sulfuric acid as an important removal process. *Environ. Sci. Technol.* **51**, 8422–8431 (2017).
65. Elm, J. An atmospheric cluster database consisting of sulfuric acid, bases, organics, and water. *ACS Omega* **4**, 10965–10974 (2019).
66. Ma, F. et al. Piperazine enhancing sulfuric acid-based new particle formation: implications for the atmospheric fate of piperazine. *Environ. Sci. Technol.* **53**, 8785–8795 (2019).
67. Shen, J. et al. Methanesulfonic acid-driven new particle formation enhanced by monoethanolamine: a computational study. *Environ. Sci. Technol.* **53**, 14387–14397 (2019).
68. Shen, J. et al. Structural effects of amines in enhancing methanesulfonic acid-driven new particle formation. *Environ. Sci. Technol.* **54**, 13498–13508 (2020).
69. Zhang, R., Shen, J., Xie, H.-B., Chen, J. & Elm, J. The role of organic acids in new particle formation from methanesulfonic acid and methylamine. *Atmos. Chem. Phys.* **22**, 2639–2650 (2022).
70. Luchini, G., Alegre-Requena, J. V., Funes-Ardoiz, I. & Paton, R. S. GoodVibes: automated thermochemistry for heterogeneous computational chemistry data. *F1000Research* **9**, 291 (2020).
71. Jen, C. N., Hanson, D. R. & McMurry, P. H. Toward reconciling measurements of atmospherically relevant clusters by chemical ionization mass spectrometry and mobility classification/vapor condensation. *Aerosol Sci. Technol.* **49**, i–iii (2015).
72. Thomas, J. M. et al. Ion mobility spectrometry-mass spectrometry examination of the structures, stabilities, and extents of hydration of dimethylamine-sulfuric acid clusters. *Phys. Chem. Chem. Phys.* **18**, 22962–22972 (2016).

ACKNOWLEDGEMENTS

The work is supported by the National Natural Science Foundation of China (22188102 and 21876024), the National Key Research and Development Program of China (2022YFC3701000, Task1), the Academy of Finland (332547, 337549, 302958), Samsung PM_{2.5} SRP, the Independent Research Fund Denmark (Grant No. 9064–00001B), US Department of Energy (DE-SC0021208), the US National Science Foundation (CHE-2004066), Supercomputing Center of Dalian University of Technology, and Center for Scientific Computing, Aarhus (<http://phys.au.dk/forskning/cscaa/>).

AUTHOR CONTRIBUTIONS

H.-B.X., J.J., and J.E. designed the research; R.C., H.-B.X., and J.J. wrote the paper with inputs from other co-authors; R.C., R.Y., D.X., M.K., J.Z., and J.J. collected measurement data; X.L., J.C., H.-B.X., and J.E. performed theoretical computations; R.C., R.Y., and L.X. analyzed data with the help from H.-B.X., V.-M.K., J.N.S., Y.M., and J.J.

COMPETING INTERESTS

The authors declare no competing interests.

ADDITIONAL INFORMATION

Supplementary information The online version contains supplementary material available at <https://doi.org/10.1038/s41612-023-00405-3>.

Correspondence and requests for materials should be addressed to Hong-Bin Xie or Jingkun Jiang.

Reprints and permission information is available at <http://www.nature.com/reprints>

Publisher's note Springer Nature remains neutral with regard to jurisdictional claims in published maps and institutional affiliations.



Open Access This article is licensed under a Creative Commons Attribution 4.0 International License, which permits use, sharing, adaptation, distribution and reproduction in any medium or format, as long as you give appropriate credit to the original author(s) and the source, provide a link to the Creative Commons license, and indicate if changes were made. The images or other third party material in this article are included in the article's Creative Commons license, unless indicated otherwise in a credit line to the material. If material is not included in the article's Creative Commons license and your intended use is not permitted by statutory regulation or exceeds the permitted use, you will need to obtain permission directly from the copyright holder. To view a copy of this license, visit <http://creativecommons.org/licenses/by/4.0/>.